Separation efficiency and ice strength properties in simulated natural freezing of aqueous solutions

John Miia, Suominen Mikko, Kurvinen Emil, Hasan Mehdi, Sormunen Otto-Ville, Kujala Pentti, Mikkola Aki, Louhi-Kultanen Marjatta

DOI: 10.1016/j.coldregions.2018.11.006

Separation efficiency and ice strength properties in simulated natural freezing of aqueous solutions

Miia John[a,*], Mikko Suominen[b], Emil Kurvinen[c], Mehdi Hasan[a], Otto-Ville Sormunen[b], Pentti Kujala[b], Aki Mikkola[c], Marjatta Louhi-Kultanen[a,d]

[a]*Separation and Purification Technology, LUT School of Engineering Science, Lappeenranta University of Technology, P.O. Box 20, FI-53850 Lappeenranta, Finland*
[b]*Department of Mechanical Engineering, School of Engineering, Aalto University, P.O. Box 15300, FI-00076 Aalto, Finland*
[c]*Department of Mechanical Engineering, LUT School of Energy Systems, Lappeenranta University of Technology, P.O. Box 20, FI-53850 Lappeenranta, Finland*
[d]*Department of Chemical and Metallurgical Engineering, School of Chemical Engineering, Aalto University, P.O. Box 16100, FI-00076 Aalto, Finland*

Abstract

In geographical regions with sub-zero temperatures, natural freezing can potentially be used as an energy-efficient purification technique for industrial wastewaters. The utilization of this technique requires knowledge of the effect of impurities on the strength of the ice to enable the effective harvesting of produced ice. Previous studies of the mechanical properties of model-scale ice have tended to focus on the initial solution, and little consideration has been given to the amount of impurities trapped inside the ice. The aim of this research is to evaluate the separation efficiency during the natural freezing process by quantifying the impurities trapped inside the ice formed from known concentrations of aqueous solutions and to investigate the effect of impurities on the bulk mechanical properties of the ice.

In this study, twenty similar size ice beams were prepared in freezing boxes in a temperature-controlled cold room from five different aqueous solutions – tap water, and ethanol and sodium chloride aqueous solutions of two different molalities, i.e. 0.1 mol/kg and 0.3 mol/kg. The

* Corresponding author.
E-mail address: miia.john@lut.fi

bending strength and natural frequencies of the ice samples were measured in the freezing conditions, and the concentrations of impurities in melted ice samples were determined. The research shows that with the ethanol and sodium chloride solutions, the concentration of impurities inside the ice clearly decreased in comparison to the initial solution. The structure of the ice from the different solutions differed significantly; as the tap water formed columnar ice, ethanol ice grew through large platelets, while the structure of the sodium chloride ice was a mixture of the two forms. The tap water yielded the highest strength ice and the ice formed from the ethanol aqueous solutions the weakest ice. The measurements indicated that the concentration of impurity in the ice reduces the mechanical strength and the magnitude of the effect varies with the chemical characteristic of impurity.

Keywords: Flexural strength; Ice purity; Natural freezing; Natural frequency

1 Natural freeze crystallization and mechanical properties of ice

The insufficiency of accessible water and worsening of water quality due to industrial discharges have made it necessary to find alternative and energy efficient water purification methods. The conventional processes to treat wastewaters are adsorption, chemical precipitation, electrolytic treatment, flotation, ion exchange, and membrane filtration, which all have unique properties and suitable water types. Natural freezing is an alternative method to achieve purification. When freezing is implemented in a wastewater basin under natural weather conditions, the cooling energy of arctic sub-zero temperature regions can be utilized to energy efficient wastewater treatment. A pure ice layer is forming over the wastewater basin similar way as in lakes, rivers and seas. A conceptual approach for wastewater purification by natural freezing is presented in Fig. 1.

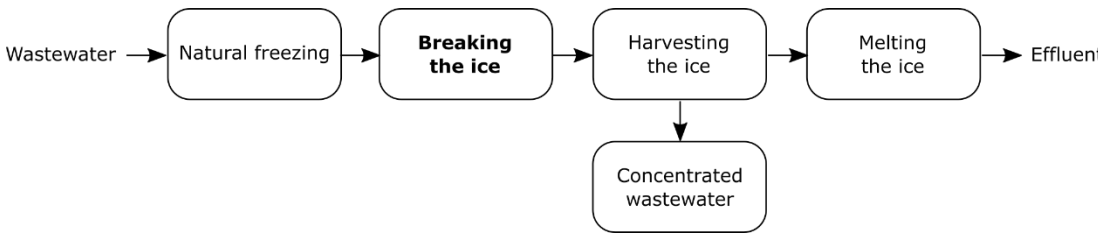

Fig. 1 Conceptual approach for wastewater purification by natural freezing.

During the freezing of a solution, heat of crystallization is released into the surroundings. The ice crystal lattice usually rejects solute molecules/ions because of their excessive size, preventing the formation of a solid solution with water (Petrich and Eicken, 2010). Thus, solutes redistribute during ice crystallization. The extent of the redistribution is attributed to the capability of the solute to diffuse away from the ice-solution interface (Butler, 2002). Succeeding these points of view, the temperature and concentration gradients are created adjacent to the growing ice front (Butler, 2002; Hasan and Louhi-Kultanen, 2015). Sea ice is a paradigm of natural freezing. The main source of impurity in sea-ice is the formation of brine pockets within the ice matrix (García et al., 2014). Analogously, the impurity of ice forming from any type of solution could be interpreted by the entrapment of the freeze concentrated solution in the ice crystal lattice. The efficiency of natural freezing is influenced by solution concentration and different growth conditions, such as the ambient temperature, freezing time and freezing rate. The effect of these factors on ice purity is epitomized by ice formation from sodium sulphate solutions. Experimental results show that a lower growth rate and solution concentration are in favour of higher ice purity (Butler, 2002).

The mechanical properties of ice have been the interest of research in glaciology and geosciences for decades (Schulson and Duval, 2009) and many different methods have been utilized in various studies. The dynamic modulus of elasticity of freshwater and saline ice has been studied by Snyder et al. (2016) with ultrasonic measurement. The effect of porosity on

the dynamic modulus of elasticity found to be aligned with earlier researches (Snyder et al., 2015; Schulson and Duval, 2009). Yasui et al. (2017) used a three-point bending test for determining the fracture toughness of ice. The Acoustic Emission (AE) was utilized to detect failure in a cyclic test of ice (Hammond et al., 2018). The effects of various mixtures of compounds on formed ice have also been an interest of studies. Recent research has been focused on studying the effect of freshwater ice and silica mixture on the mechanical properties of ice (Yasui et al., 2017) and sulfuric acid doped ice under tension and compression (Hammonds and Baker, 2018). The effects of Ca++ doped ice to the ice strength (Hammonds and Baker, 2016) and the mechanical properties of saline ice (Snyder et al., 2016) have been studied as well.

The strength of sea ice and parameters affecting the strength have been the object of study for decades. In terms of impurities, the salinity (through brine volume) has been observed to have a clear effect on the mechanical properties of ice, see e.g. Timco and O'Brian (1994) for the flexural strength and Timco and Weeks (2010) for modulus of elasticity. Timco and O'Brien (1994) have combined several databases and shown that the flexural strength can be determined based on the square root of the brine volume, which can be determined based on temperature and salinity. Values over 1.5 MPa have been measured for the flexural strength of first-year sea ice, but values typically range from 1 MPa and decrease with the brine volume, being of the order of 100 to 150 kPa for warm sea ice (Timco and Weeks, 2010). The estimates for the flexural strength of old ice, i.e. second year and multiyear sea ice, would be of the order of 0.8 to 1.1 MPa in the winter and 0.4 to 0.6 MPa in the summer (Timco and Weeks, 2010). In the Baltic Sea, the four-point bending tests have shown the flexural strength to be 0.58 MPa on average and from 0.42 MPa to 0.55 MPa when determined form cantilever beam tests (Enkvist, 1972; Määttänen, 1976; Kujala et al., 1990).

In addition, the studies have shown that the brine volume has a clear effect on the elastic and static modulus. The elastic modulus here refers to Young's modulus (*E*) determined with dynamic measurements and a static modulus to Young's modulus determined from static tests. The dynamic measurements are commonly determined by measuring the rate of wave propagation in ice or by exciting the natural resonant frequencies of different vibration modes (Weeks and Hibler, 2014). The experimental results have shown that the values of the elastic modulus vary between 1.7 and 5.7 GPa when determined from flexural waves, and from 1.7 to 9.1 GPa when determined from body-wave velocities (Weeks and Assur, 1968). Anderson (1958) has shown that there is a clear decreasing trend in the elastic modulus as a function of brine volume. The static modulus for sea ice has been commonly determined from the bending tests (see e.g. Dykins, 1971). Similar to dynamic tests, the static tests have shown that the static modulus decreases as a function of brine volume (see e.g. Vaudrey, 1977). The static modulus measurements have shown a great scatter and the values have been, on average, between 1 and 5 GPa (Timco and Weeks, 2010). For more detailed discussions on the effect of brine volume and other environmental factors on the elastic and static modulus of sea ice, see (Borland, 1988; Hirayama, 1983; Lau et al., 2007; Lehmus, 1988; Nortala-Hoikkanen, 1990; Riska et al., 1994; Weeks and Hibler, 2014).

Besides salt (sodium chloride), the development of model scale ice has raised interest towards the effect of other chemicals on the strength of ice. The general conclusion is that adding these dopants to the water weakens the formed ice in terms of flexural strength (e.g. Borland, 1988), and the elastic modulus (Hirayama, 1983). As the flexural strength has been considered the most important mechanical property of ice for ship model scale testing, the development has focused on scaling the flexural strength correctly and then confirming that the ratios between

other parameters are in the same range as with sea ice. Due to the typical size of the ships with respect to the size of the model scaled ships, the typical scale ratio for the model is 10 to 40, and thus, the required flexural strength is from 15 kPa to 60 kPa in model scale (Lau et al., 2007). Therefore, the minimum for the ratio between the static modulus and the flexural strength is 2000, and it can reach a value of 8000 (see e.g. Riska et al., 1994; Timco, 1980).

Timco (1981) conducted the most extensive flexural strength tests with different chemicals. The chemicals included acetates, amides, various inorganic salts as well as sucrose with fixed mass fractions (Timco, 1981). Timco (1981) compared the influence of various mass fractions of the selected chemicals on the flexural strength of ice. The higher mass fractions led to lower flexural strength of ice (Timco, 1981). Furthermore, different model scale basins have ended up using different chemicals, which include urea, a mixture of ethylene glycol, aliphatic detergent and sugar (EG/AD/S), alcohol and sodium chloride (see e.g. Borland, 1988; Hirayama, 1983; Lau et al., 2007; Riska et al., 1994; Lehmus, 1988; Nortala-Hoikkanen, 1990), for studies with different types of model scale ice. The measurements have shown that with these chemicals combined with different ice production methods (seeding or spraying) the flexural strength can be scaled to 15-60 kPa with different solutions (Lau et al., 2007). However, the measurements have shown that the ratio between the elastic modulus and the flexural strength of the urea doped model ice is $\leq$ 2000 (Hirayama, 1983; Narita et al., 1988). The range for EG/AD/S doped ice is 1000–3000 (Timco, 1986) and for the correct density (CD)-EG/AD/S 2000–3250 (Lau et al., 2007). The fine-grained ethanol ice, however, covers the ratio range of 1750–5000 (Riska et al., 1994).

However, in the development of the model scale ice, the interest is commonly in the initial

143 solution and freezing process. Thus, the studies generally account for the mass concentration
144 of the chemical in the initial solution and neglect how much of the chemical is trapped inside
145 the ice, i.e. the amount of chemical actually affecting the properties of the ice. These
146 simplifications are usually for practical reasons (it is easier to observe and control the mass
147 concentration of the initial solution and then check the obtained mechanical properties).
148 Furthermore, due to the weakening effect of chemicals, the model scale ice is difficult to move
149 from in-situ without damaging it. Thus, the static modulus is commonly determined from the
150 plate deflection and the flexural strength is determined from a cantilever beam test, as
151 recommended by ITTC guidelines (ITTC guidelines, 2014). In addition, the dynamic
152 measurements are conducted with a scanning laser Doppler vibrometer (SLDV) to measure
153 the natural frequencies (Polytec, 2017).
154
155 The natural frequencies of the ice indicate the internal structure dynamic behaviour for a
156 known geometry, i.e. an ice beam. They can be considered a measure determining the
157 mechanical dynamic property of the ice. (Rao, 2007). The formed ice beams consisted of many
158 interconnected different shaped, sized and oriented ice crystals. In this study, the complete
159 ice beam dynamics response was measured. The ice in solid form was then assumed to
160 behave like a solid particle, where the natural frequencies of a solid particle are fundamentally
161 related to the square root of mass divided by stiffness (Carvill, 1994). Knowing the natural
162 frequencies of an ice sample allows calculating the equivalent modulus of elasticity, i.e. the
163 overall stiffness, which is important to know when modelling the sample that has the same
164 dynamical behaviour as the actual formed ice. Calculating the modulus of elasticity requires,
165 in addition, knowledge of the ice sample's physical dimensions, density and area moment of
166 inertia. For a beam shaped ice piece, the modulus of elasticity can be analytically calculated.
167 The assumption is that the impurities captured in the ice have an impact on the stiffness of the

ice and thus the impurities could be detected from the natural frequencies. The ice can be excited at natural frequencies, which causes energy to collect in the ice and the ice to yield and break into smaller parts.

In the application of wastewater purification by freezing, measuring and determining the mechanical properties of ice are important. This information can be used to estimate the ice strength and to evaluate the needed force for breaking and collecting the ice in a purification process application. Analysing the ice strength by the four point bending test has been found to be accurate and commonly used method (Kujala et al., 1990). Compared with the three point bending test, the shear force does not change rapidly in the location where the failure is assumed to occur, i.e. in the middle of the loaded beam, as can be seen from beam theories, see e.g. (Parnes, 2001). The advantage of using simple beam tests over the cantilever beam tests is that root stresses do not disturb the measurements by lowering the measured flexural strength values as noted by Timco and O'Brian (1994). The information about the ice mechanical rigidity can be gained through measuring the natural frequencies. Natural frequencies can be measured without breaking the ice sample e.g. by exciting the ice externally, recording the velocity response and post-processing it. Natural frequencies can be detected with non-contact and non-destructive method, which is beneficial for detecting the ice mechanical rigidity.

Hence, the aim of this research is to determine the amount of ethanol and sodium chloride trapped inside the laboratory-produced ice and their effect on the mechanical properties of the ice: the flexural strength, static and dynamic elastic modules. These parameters are required when designing a wastewater purification apparatus and testing the performance of ice breaking vessels.

2 Freezing test procedure

To our best understanding, the chemical quantity in the solution determined by the molality (moles of chemical per kg of water) is a better measure for the comparison of chemical impacts than using the mass percent (wt-%) based quantity due to the different molar masses of the studied chemicals. The molar mass of sodium chloride NaCl, 58.443 g/mol, is much higher than the molar mass of ethanol C_2H_5OH, 46.068 g/mol (Haynes, 2017). Due to this fact, in the present work we fixed the solute quantities based on molality (mol chemical/kg tap water). In this study, five different solutions were prepared: tap water (basic liquid), two organic aqueous solutions and two inorganic aqueous solutions, both with two different molal concentrations, 0.1 mol/kg and 0.3 mol/kg. The initial solution was mixed in a 100 kg batch. The solutions were prepared in room temperature and an agitator was used to achieve sufficient mixing during dissolution. The initial aqueous ethanol solutions were prepared by dissolving ethanol (ETAX B16 with 92.4% ethanol content supplied by Altia Industrial) in tap water. The initial aqueous sodium chloride solutions were prepared by dissolving 99.9% pure sodium chloride (supplied by VWR Chemicals) in tap water. The tap water was high-quality drinking water with a temperature of 13 - 15 °C at that time. The quality of water is guaranteed by the water supplier and contains very low concentrations of impurities due to requirements. Samples of 500 ml from every five initial solutions were obtained after preparation. The solutions were carried in lidded containers to a cool storage where they awaited further test preparation.

After the solutions were prepared, each batch was divided into four freezing boxes made of insulated material, Finnfoam (housing insulation material, polystyrene), to prevent freezing on the sides and bottom, i.e. the cold was affecting the surface layer while the foam walls insulated the sides and bottom, thus replicating natural freezing. Therefore, the heat flux

migrated mainly from the solution through the ice layer to cooling air. In total, twenty similar freezing boxes were used in the freezing experiments. The boxes consisted of outer and inner boxes. The utilization of two boxes allowed removing of the ice sample with low effort, as the ice could be taken out easily by lifting the inner box with the sample. The inner dimensions of the inner boxes were 60 cm in length and 15 cm in width. The depth of the inner box was lower than the depth of the outer box, as the aim was to freeze half of the solution in maximum. Thus, the separation efficiency of natural freezing could be kept at moderate level when less than 50% of solution is frozen (Hasan and Louhi-Kultanen, 2016).

The interior of the outer freezing box was lined with plastic to make the box waterproof. The open section between the inner and outer boxes was insulated by placing a piece of joint insulation foam, commonly used in buildings, between the boxes. Thus, it prevented the boxes from freezing together. An elastic rope was placed into the box to mount the frozen samples for the natural frequency measurements. Prior to pouring the solutions, each box was weighed with a Sartorius LC 34000P balance (capacity 34 kg and readability 0.5 g). Each sample contained 24 kg of the initial solution and was weighed in room temperature.

After all of the boxes were prepared, weighed and filled with solutions, the boxes were taken into the cold room, where the targeted temperature was -5 ºC. The samples were placed in the room in a four by five matrix form where each column formed a line of similar initial samples. The first row of solutions was closest to the door and the fourth row closest to the back wall. Fig. 2a shows the arrangement and naming of the samples. The naming is in sequential order. The first letter “P” refers to the tap water, “E” to the ethanol solution and “S” to the sodium chloride solution. The preceding numbers 1, 2, 3 and 4 represent the row number. The third item refers to the molality: “a” to 0.1 mol/kg and “b” to 0.3 mol/kg. The fourth

letter refers to the ice section: “t” to the top (upper) section of the ice, “c” the centre section and “b” the bottom section. In the results, the naming labels, e.g. “E1at” refers to ethanol solution, row 1, molality of 0.1 mol/kg and top section. Fig. 2b shows the freezing arrangement in the cold room.

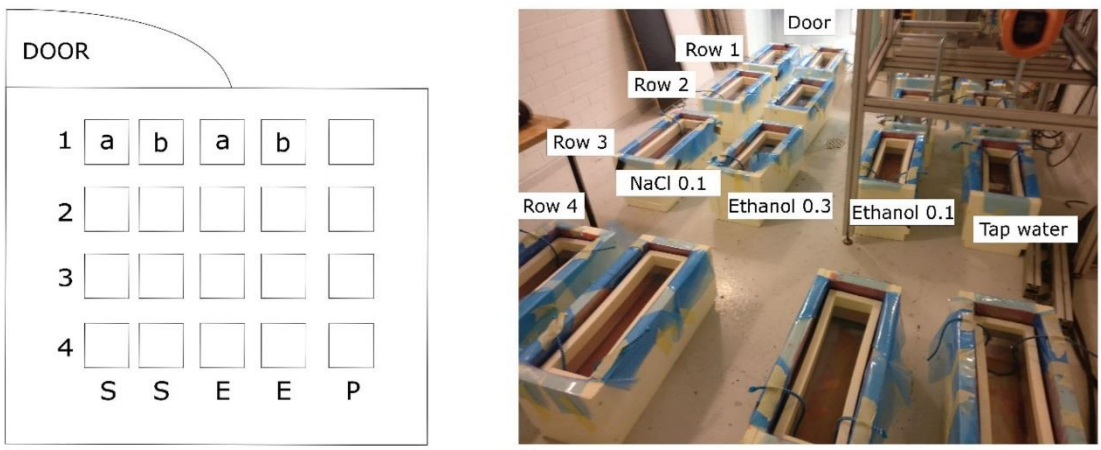

a) b)

Fig. 2 Freezing arrangement. a) Layout of freezing boxes. b) Picture taken in the cold room (NaCl 0.3 has not been carried in yet).

A temperature sensor was placed in each box in the first row to monitor the temperature in the liquid during freezing, and in addition, the ambient temperature was measured from the middle of the first row. A total of six PT100 thermometers were connected to two PicoLog PT-104 data loggers, which were connected via USBs to a laptop.

2.1 Natural frequency

The natural frequencies were measured in the cold room to avoid the melting of the ice samples. The measurement was conducted with an optical scanning laser Doppler vibrometer (SLDV). The SLDV is a non-contact and non-destructive method of measuring surface velocities and consequently natural frequencies. The optical signal allows measuring through transparent media, e.g. glass or water. It is based on the Doppler effect and measures the

surface velocity of excited ice. (Polytec, 2017). In practice, the laser signal is focused on a predefined plane, which is the front of the measured sample. An example of using SLDV for measuring through a glass window into a water tank to measure an ultrasonic transducer far-field characteristics can be seen from Cooling et al. (2010).The ice was excited with a piezo exciter (PI P-844.10) and the frequency response was recorded at given locations. To be able to record the reflective laser signal, a 10 mm wide retroreflective tape (A-RET-T010) was attached by freezing with a small amount of 0 °C tap water vertically on the upper surface of the ice. The possible detrimental effect of the retroreflective tape on the dynamic motion of the measurements can be neglected as the thickness of the tape (0.1 mm) is very small in comparison with the ice thickness (minimum ~30 mm). In addition, the small amount of water to bond the tape on the ice is so thin that the effect on dynamics is negligible.

The ice was hung with elastic rope, which was placed in the solution prior to freezing. There is a large difference in the stiffness of the ice and the elastic rope with which it is hung. This enables capturing only the ice internal dynamical behavior. The ice samples were also supported from the bottom to limit the rigid body motion. Fig. 3a depicts the hardware located outside the cold room: a Polytec PSV-500 scanning head and an OFV-505 reference laser pointed directly at the glass window. Fig. 3b depicts the ice hanging setup inside the cold room. The measurement procedure has three initial steps. The first is to set a measurement plane, that is in this case the top surface of the ice beam. Secondly, the visible laser is focused on the top of the plane. Thirdly, the 3D orientation is defined by the origo, Y-direction and XY-plane. The scanning hardware operation temperature is limited to the range of +5 to +40 ºC; thus, the measurement was conducted through the transparent glasses. The piezo exciter's operating temperature is limited to -20 to +80 ºC, and it could thus be used in the cold room to excite the ice sample. The exciter is made from steel and was stored in the cold room to avoid

melting the ice sample when in contact with it. Fig. 3c depicts the front surface of the ice sample. The ice pieces that were strong enough to hang from the flexural rope were measured. The natural frequencies were measured from the upper surface of the ice and the excitation was given from the bottom layer.

Fig. 3 Setup for measuring natural frequencies of the ice samples: a) Polytec vibrometer unit outside of the cold room b) ice sample hanging with flexible ropes and stabilized in the bottom with additional flexible ropes. c) Retroreflective tape frozen to the front surface of the ice.

The modulus of elasticity (via dynamic measurement) E_d is calculated based on beam theory

$$E_d = \frac{(f_n \cdot 2\pi)^2 \cdot A \cdot \rho \cdot L_B^4}{k^4 \cdot I}, \quad (1)$$

where f_n is the natural frequency, A is the cross sectional area, ρ is the ice density, L_B is the ice beam length, k is a factor dependent on the support. For free-free supported body, i.e. freely floating body, as is in this case, the factor for the first flexural natural frequency is 4.730, and I is the area moment of inertia. (Rao, 2007).

2.2 Flexural strength

The flexural strength of ice was measured with a four-point bending test in the cold room. Fig. 4 presents the test setup. The test sample was placed on top of the rounded wooden supports.

The two load sensors were mounted with an aluminium profile onto the electrically driven piston. The load sensors were HBM S2M 500N. Rounded wooden parts were attached under the sensors, which were in contact with the ice beam in the loading. The rounded wood pieces allow rotational movement in the ice under loading. In each test, the displacement was measured at the mid span of the ice beam with HBM WA 10 mm displacement sensors. The forces and displacement were recorded with a frequency of 1.2 kHz.

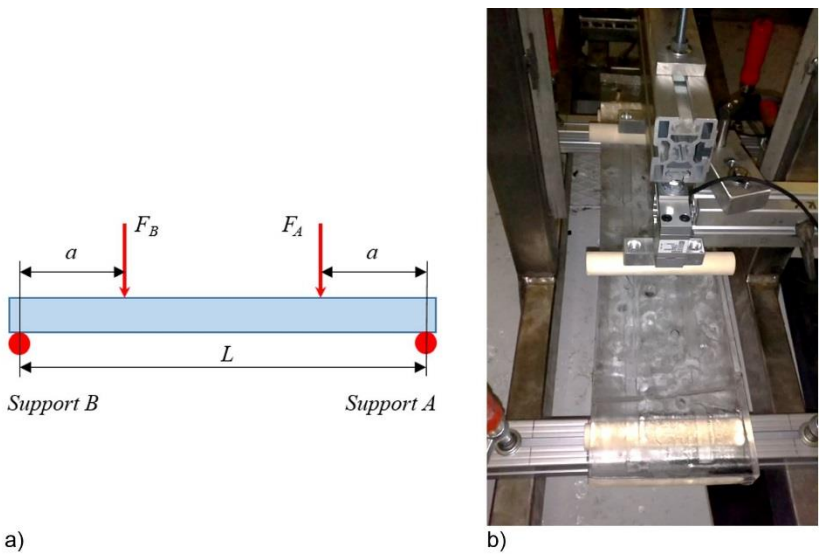

a) b)

Fig. 4 Four-point bending test setup. a) The principle picture from the test. b) The device measuring the P4 ice sample.

After the loading, the distance of the breaking point was measured from the left-hand side support. In addition, the thickness and the width of the ice beam at the breaking point were measured. The ice beam is assumed to behave as an Euler-Bernoulli beam. At first, the moment equation along the beam is determined from the free-body diagram. It is assumed that the first failure in a bending situation occurs on the surface in tension, as the axial stress (in the longitudinal direction) maximum occurs on the surface of the beam. Knowing the relation (Parnes, 2001):

$$\sigma_x = \frac{My}{I} \tag{2}$$

where σ_x is the axial stress, *M* is the moment affecting the cross-section, *y* is the distance from the neutral axis, and *I* is the second moment of inertia. Inserting the moment equation in this equation we obtain the following form for the flexural strength (σ_f):

$$\sigma_f = 3 \cdot \frac{(L-x)\cdot x\cdot \rho\cdot g}{h} + 6\,\frac{(L-x)\cdot a\cdot F_B + a\cdot x\cdot F_A}{L\cdot b\cdot h^2}, \tag{3}$$

where L is the distance between the supports, x is the distance of the crack from the left-hand side support, g is the gravitational acceleration, h is the thickness of ice, *a* is the distance of a sensor from the same side support, F_A is the load measured with the right load sensor, F_B is the load measured with the left load sensor, b is the width of the sample.

2.3 Static modulus of elasticity

The displacement was measured simultaneously with the force. This enables the determination of the static modulus of elasticity (E_s), i.e. the effective Young's modulus. In this case, the ice beam is assumed to behave as an Euler-Bernoulli beam. After the moment equation along the beam is determined, the displacement equation, *w*, for the beam can be derived from the following relation (Parnes, 2001):

$$EI\frac{d^2w}{dx^2} = -M(x). \tag{4}$$

After the displacement equation is determined and the displacement is measured from a

known location, the static modulus (E_s) of elasticity can be determined from the following equation:

$$E_s = \frac{(34 \cdot a \cdot L^2 - 64 \cdot a^3) \cdot F_B + 16 \cdot a \cdot L^2 \cdot F_A}{384 \cdot I \cdot w_{centre}}, \quad (5)$$

where the second moment of inertia (I) was determined by measuring the width and the height of the tested beam from the location the failure occurred and w_{centre} is the width at the failure location. This assumes the beam is solid with negligible porosity and uniform thickness and the width of the beam over the length.

Unfortunately, some of the ice beams were broken when taken out from the freezing boxes. 4 of 30 beams (or halves) broke before the measurements. The fourth row of ice was mainly too weak for the bending strength test. Row 2 ice was measured as full beams. Rows 1 and 3 ice beams were cut in half for the bending test and static modulus of elasticity. Due to the test set-up, it was not possible to mount the displacement sensor on the rig for samples broken when taken out from the freezing boxes, as the span between the supports was small.

2.4 Chemical analyses

The formed ice layer and concentrated residual solution under the ice layer were separated after the freezing test period by lifting up the ice layer from the freezing box. The total mass of the ice layer was weighed and the ice was moved to mechanical testing. A 500 ml sample was taken (after agitating the liquid) from the concentrated solution remaining in the box. After the mechanical tests of ice (the frequency measurement and flexural strength test), the ice samples for chemical analysis were collected within various horizontal layers sliced in sections of 1 to 4 cm thicknesses using a band saw. The ice pieces were rinsed with purified water, produced by Elga PureLab water system (resistivity 18.2 MΩ·cm, TOC < 5 ppb) to avoid

external contamination during the ice handling. Composite ice samples from a layer were collected into a plastic bag for crushing with a hammer. The crushed ice was packed tightly in 250–500 ml polyethylene bottles for freeze storing, transporting and further chemical analysis. The total amount of samples was 70: 5 initial solution samples, 20 concentrated solution samples, 10 whole ice layer section cut samples and 35 ice layer samples from different horizontal layers. Furthermore, vertical and horizontal ice layer samples were cut and collected from the ice samples in rows two and three to visually observe the crystal structure by placing the samples between two polarizing films and directing light through the arrangement.

All freeze stored samples were melted at room temperature. The samples containing tap water and ethanol were analyzed with a total organic carbon (TOC) analyser (Shimadzu TOC-L + ASI-L Autosampler, detection limit 4 µg/l) to determine the concentration of total organic carbon. Ethanol concentrations were further calculated based on TOC concentrations. Molar mass of ethanol C_2H_5OH is 46.068 g/mol, of which 52.50% is carbon (Haynes, 2017). Electrical conductivities of samples containing tap water and sodium chloride were measured by a Consort C3040 Multi-parameter analyser with conductivity electrode SK20T (range 1.0 µS/cm to 100 mS/cm, cell constant 1.0 1/cm). Sodium chloride concentrations were determined by linear fitting based on conductivity values reported in literature (Haynes, 2017). The densities of all samples (melted ice, initial solution and concentrated solution) were determined by an Anton Paar DMA4500 density meter (repeatability with density $1 \cdot 10^{-5}$ g/cm^3 and temperature 0.01 °C). NaCl and ethanol concentrations were determined by linear fitting based on density values reported in literature (Haynes, 2017).

3 Results

3.1 Temperature profile

The temperatures were recorded from the first row samples with an interval of one minute until the samples in the second last row (row 2) were taken out from the freezing boxes. Fig. 5 depicts the logged temperature profile, and the vertical lines indicate the times of ice removal from the boxes. At first, the cooling rates varied considerably due to the diverse temperatures of the liquids when the cooling and freezing started. After 45 h of freezing, temperatures of liquids attained final constant temperatures. Tap water, the 0.1 mol/kg NaCl solution and the 0.3 mol/kg NaCl solution stayed at temperatures -0.03 °C, -0.33 °C and -1.07 °C, respectively, and were close to known freezing point depression (FPD) temperatures ~0 °C, -0.34 °C and -1.02 °C reported in literature (Haynes, 2017). The ethanol 0.1 mol/kg solution appeared slightly undercooled with a temperature of -0.28 °C when the FPD temperature is -0.17 °C (Haynes, 2017). The 0.3 mol/kg ethanol solution was rather warm with a temperature of -0.42 °C when compared to the FPD temperature of -0.54 °C (Haynes, 2017). Unexpectedly, this concentrated ethanol solution also started to cool down after 70 h of freezing, when the temperature of the freezing room was decreased and the solution reached an undercooled temperature of -1.7 °C. The temperature probe used for the 0.3 mol/kg sodium chloride solution shows a colder temperature after 70 h, as it was accidentally pulled out from the solution and exposed to the cold room temperature. The aim was to seed the solutions prior to ice forming. However, after ten hours, it was noted that frazil natural ice formed on the surface of tap water and 0.1 mol/kg ethanol solutions as well as rows three and four of 0.3 mol/kg ethanol solutions. Thus, these samples were not seeded, whereas all the sodium chloride solutions and ethanol solutions E1b and E2b were.

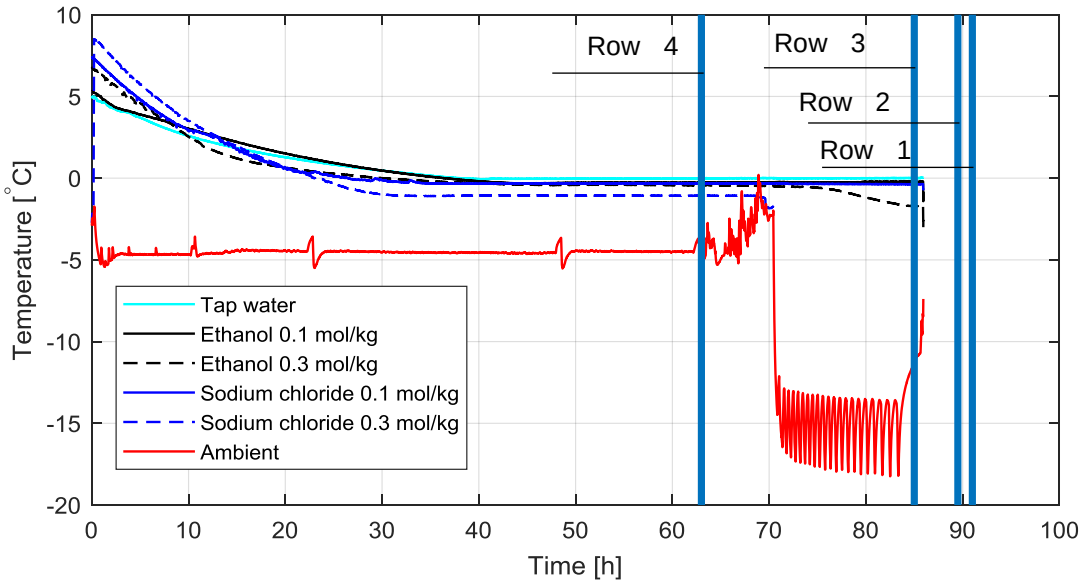

Fig. 5 Freezing temperatures and actions conducted during the measurement. Vertical lines represent the removal of each row of ice.

The samples in row four were taken out after 53 h of freezing at -5 ºC. However, the samples were rather thin (P4 35 mm, E4a 12 mm and E4b 9 mm, S4a 22 mm and S4b 19 mm). The S4a and P4 samples were the only ones rigid enough to be hung from the flexural rope for the elastic modulus measurements. Then, the ice growth continued in other rows at lower temperatures for longer freezing times to produce thicker ice layers for mechanical testing purposes. The temperature was first lowered to -15 ºC for 13 h, and after that raised to -10 ºC. As a result, the samples in row three were taken out after 75 h of freezing, of which 60 h was at -5 ºC, 13 h at -15 ºC and 2 h at -10 ºC. The thicknesses of the ice samples were 59 to 72 mm and the samples were strong enough for the mechanical property tests. To stop the ice growth in the two remaining sample rows, the temperature was increased to -5 ºC. The samples in rows two and one were frozen an additional 4.5 and 6 h, respectively, at -5 ºC before removal from the freezing boxes.

3.2 Properties of ice

The ice samples could be distinguished from the outlook from the surface of the ice; see row a) in Fig. 6. From the left, the first column is tap water (P) ice, which was clear and did not contain any bubbles. The second (Ea) and third (Eb) columns are the ethanol solutions that had some bubbles and were not fully transparent. The fourth (Sa) and fifth columns (Sb) are the sodium chloride solution and appear cloudy. After the samples were taken out from the freezing boxes, they were placed bottom up on an even surface to protect the fragile bottom ice crystals; see row b) in Fig. 6. After the mechanical properties of the ice were measured, vertical and horizontal thin sections were prepared from the samples; see rows c) and d) in Fig. 6.

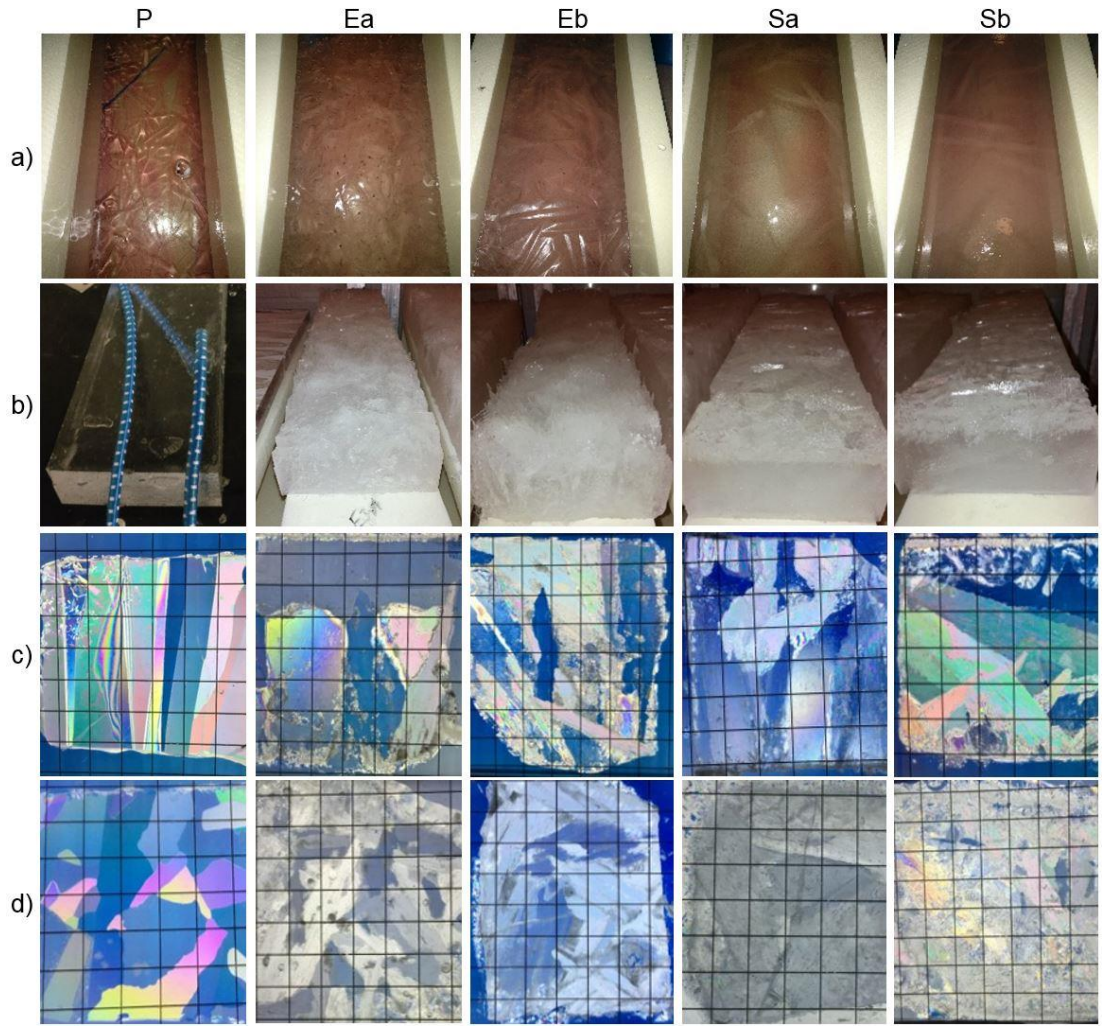

Fig. 6 Pictures of the ice samples (from row three). The columns from left to right are P, Ea, Eb, Sa, and Sb; a) the samples in the freezing boxes, b) the samples upside down after recovery, c) vertical thin sections from row two, and d) horizontal thin sections from row three. The scale bar is 1 cm x 1 cm.

The ice from tap water (P) had the most homogeneous ice crystal structure. The ice samples were clearly transparent and the top and bottom surfaces were smooth. The ice structure was columnar, with all of the crystals oriented almost vertically; see the vertical thin section in Fig. 6c) and d). However, the crystal (or grain) size in the horizontal direction varied from 10 to 40 mm and was irregular. The irregular structure is considered to result from the unseeded origin of the ice growth, as earlier studies have shown that ice with a relatively homogeneous grain

size can be obtained by seeding with ice crystals (Gow et al., 1988).

The ice grown from ethanol solutions (Ea and Eb) had the most irregular structure. The ice first grew an approximately 9 mm solid layer. After this layer, dendritic crystal platelets started to grow. The diameters of the platelets were up to 100 mm, the thickness was up to 5 mm, and the orientation appeared to be random. There were distinguished regions between the platelets, and many platelets were not connected. Fig. 7 shows the E4b sample after being taken out from the freezing box at this stage of the growth.

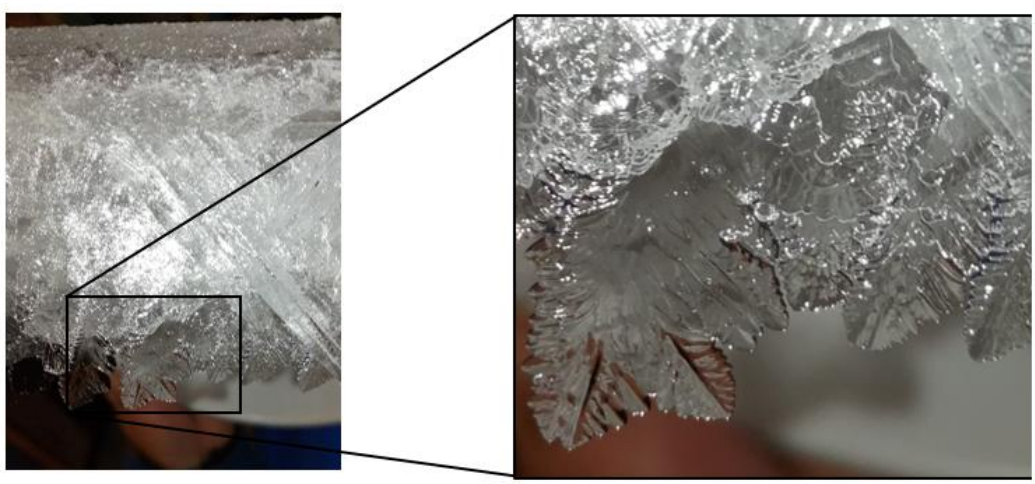

Fig. 7 Close-up of E4b ice structure from the side. On the top, approximately 9 mm of solid ice structure and then large dendritic platelets oriented towards the liquid.

When the freezing continued, bridges between the platelets started to form, leading to a more solid ice structure. However, the bottom of the ice remained irregular and thin sections showed that the gaps had not fully closed; see Fig. 6c) and d). Thus, the ice was porous, and in some cases, the platelets growing together might have entrapped ethanol solution inside the ice.

The ice from the sodium chloride solution (Sa and Sb) had a structure between the tap water and ice frozen in the ethanol solution. The ice was cloudy and almost opaque. The top surface

was smooth but the bottom surface rough. The ice grew in platelets, but thinner and smaller in diameter than in the ice obtained from the ethanol solution. The platelets were oriented locally in the same direction, see Fig. 6c) and d). The ice was also less porous than the ice obtained from the ethanol solution, as the platelets seemed to grow almost at the same rate. Thus, the ice formed in the sodium chloride solution was more solid than the ice obtained from the ethanol solution.

Prior to the mechanical and chemical measurements, the physical properties were measured. The average length of the ice samples was 567 mm and the width 143 mm. Table 1 presents the thickness, mass and growth rate of the samples. The chemical and mechanical properties were determined after physical measurements with the procedures described in Section 2. Table 1 and Table 2 present the results of the chemical and mechanical property measurements for each sample, respectively. The average ice layer growth rate ($\cdot 10^{-7}$ m/s) was calculated by the measured average ice layer thickness formed during freezing time. The average ice mass growth rate (g/h,m^2) was calculated by the mass of ice layer formed during freezing time per freezing area.

Table 1 Physical and chemical properties of the ice.

	Sample	Ice mass	Thickness	TOC	Conductivity	Calculated molality	Ice layer growth	Ice mass growth
		g	mm	mg/l	µS/cm	mol/kg H_2O	$\cdot 10^{-7}$ m/s	g/h m^2
Tap water	P1	5702 (2787[1a)])	72 (45.6[1a)])	0.7 (3.9[2)])	15 (121.8[2)])	-	2.46	823
	P2	5224	66	0.2	2.9	-	2.30	769
	P3	4801 (2473[1a)])	61 (31[1a)])	0.7	6.7	-	2.26	749
	P4	2392	31	0.9	4.0	-	1.65	528
EtOH 0.1 m	E1a	4985	71	1174 (2349[2)])	-	0.044 (0.089[2)])	2.44	720
	E2a	5079	70	1452	-	0.053	2.44	747
	E3a	4987	66	1207	-	0.045	2.45	778
	E4a	2288	29	629.8	-	0.024	1.53	505
EtOH 0.3 m	E1b	4803	75	2293 (7401[2)])	-	0.091 (0.292[2)])	2.58	693
	E2b	5095	73	2959	-	0.119	2.56	750
	E3b	4800	72	2594	-	0.103	2.66	749
	E4b	2125	27	2230	-	0.086	1.42	469
NaCl 0.1 m	S1a	5196 (2410[3)])	66 (32.95[3)])	-	2922 (9610[2)])	0.029 (0.104[2)])	2.25	750
	S2a	5212	64	-	3010	0.030	2.24	767
	S3a	5067	63	-	2894	0.030	2.34	790
	S4a	2386	29	-	1622	0.015	1.51	526
NaCl 0.3 m	S1b	5071 (2193[1c)])	63 (29.8[1c)])	-	9285 (26200[2)])	0.101 (0.302[2)])	2.17	732

	S2b	4641	59	-	7580	0.080	2.06	683
	S3b	4592	59	-	9620	0.103	2.17	716
	S4b	1983	27	-	7710	0.082	1.40	438

[1a)] Mass and thickness of the bottom ice sample when measuring natural frequency
[1b)] Average mass from the top and bottom sections when measuring natural frequency
[1c)] Mass and thickness of the top ice sample when measuring natural frequency
[2)] TOC/conductivity/molality for the initial solution
[3)] Average mass and thickness from top and bottom sections of the natural frequency measurement

466

467 **Table 2** Mechanical properties of the ice.

	Sample	Natural frequency (flexural) Hz	Flexural strength kPa	Dynamic Modulus of elasticity GPa	Static Modulus of elasticity GPa
Tap water	P1	580.80[1a)]	971.00[1d)]	7.38	-
	P2	601.00	890.00	7.93	1.27
	P3	267.10[1a)]	1384.50[1d)]	8.00	6.08[1d)]
	P4	316.50	1072.00	9.24	4.57
EtOH 0.1 m	E1a	-	366.50[1d)]	-	-
	E2a	634.50	144.00	7.22	1.12
	E3a	620.00	275.50[1d)]	7.89	1.26[1d)]
	E4a	-	-	-	-
EtOH 0.3 m	E1b	-	128.50	-	-
	E2b	-	56.00	-	-
	E3b	-	146.67	-	-
	E4b	-	-	-	-
NaCl 0.1 m	S1a	288.05[1b)]	581.00[1d)]	6.82	3.93[1d)]
	S2a	407.60	202.00	3.95	0.58
	S3a	389.40	438.50[1d)]	3.69	7.69[1d)]
	S4a	230.80	248.00	6.83	-
NaCl 0.3 m	S1b	240.50[1c)]	622.00[1d)]	5.75	4.12[1d)]
	S2b	383.00	152.00	3.98	0.57
	S3b	474.50	303.50[1d)]	6.15	5.09[1d)]
	S4b	-	-	-	-

[1a)] Natural frequency of bottom ice part
[1b)] Average natural frequency of top and bottom sections.
[1c)] Natural frequency of the top ice part
[1d)] Average value from upper and lower part

468

469 Average ice mass growth rates (g/h, m^2) of measured ice samples are plotted in Fig. 8 and

470 average flexural strength values (kPa) in Fig. 9.

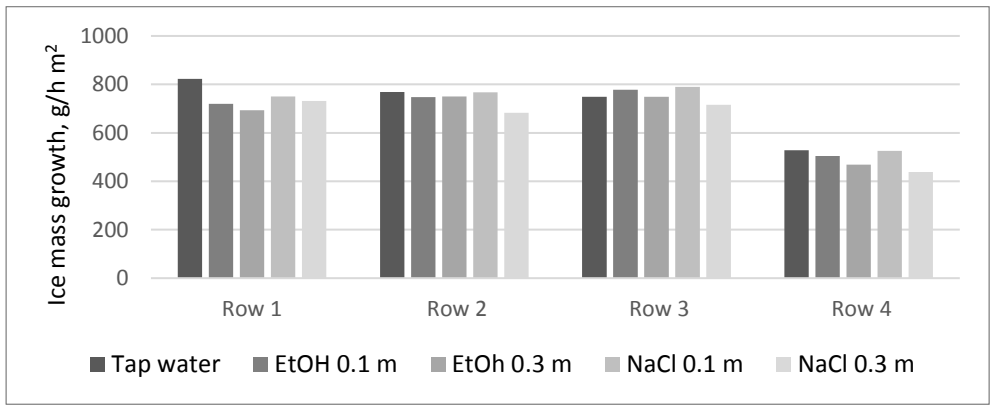

471

472 **Fig. 8** Average ice mass growth rates (g/h m^2) of measured ice samples.

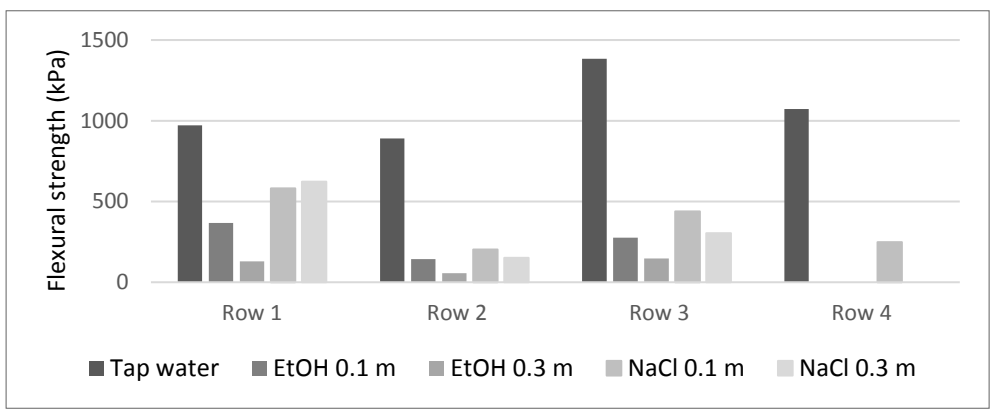

473

474 **Fig. 9** Average flexural strength values (kPa) of measured ice samples.

475

476 ## 4 Discussion

477 In the following section, the average properties of each measurement are calculated from the
478 samples of rows one, two and three, and results are compared. The samples of the fourth row
479 were taken out first when the amount of ice was still very low and mechanical measurements
480 could not be performed with three ice samples out of five.

4.1 Average ice properties of the tap water

Table 3 summarizes the average properties of tap water ice samples one to three. If the properties for the top and bottom layer were measured separately, the average of the layer measurement was used as a value for the sample. The tap water ice properties were measured for reference values to compare the difference in the ice structures grown in ethanol and sodium chloride solutions. As the ethanol and sodium chloride were mixed with the tap water, the effect on its properties was captured. The average mass of ice that was created was 5242 g, and the measured density was 934 kg/m^3. The natural frequency is related to the thickness of the ice, as the width and length of the beams were identical. This gives a value for the stiffness of the ice that formed in relation to the thickness of the ice. The higher the value for Hz/mm is, the stiffer the formed ice layer is. The modulus of elasticity is calculated from the first flexural natural frequency and beam theory (Eq. 1). The static modulus of elasticity is calculated from the displacement during the flexural strength test that is based on a static test (Eq. 5). In addition, the flexural strength was measured for the created ice samples. The ice formed from the tap water has the highest natural frequency per thickness, modulus of elasticity and flexural strength; compare Table 3, Table 4 and Table 5.

Table 3 Averafge ice properties of the tap water samples one to three.

Property	Unit	Tap water
Mass growth rate per unit surface area	g/h m^2	780
Linear growth rate	m/s	$2.34 \cdot 10^{-7}$
Mass	g	5242
Density	kg/m^3	934
Natural frequency	Hz	483
Thickness	mm	66.33 (47.47)[1)]
Average natural frequency per mech. thickness	Hz/mm	10.17
Dynamic modulus of elasticity	GPa	7.77
Flexural strength	kPa	1082
Static modulus of elasticity	GPa	3.68

[1)] Average thickness from natural frequency measurements

4.2 Average ice properties of the ethanol solutions

Table 4 shows the average properties for the ice grown from ethanol solutions. The ice formed from the 0.3 mol/kg solution was very weak, and only part of the measurements were possible to conduct. Compared to the tap water properties, the ice mass growth rate was lower but the ice layer growth rate was higher. The average natural frequency per thickness was lower, meaning that the ethanol ice was softer. The flexural strength was significantly lower compared to the tap water ice, which is also visible from the modulus of elasticity (static) that was determined from the four-point bending test. Table 4 shows that the ice that formed from the concentrated ethanol solution is clearly mechanically weaker, as expected. The average separation efficiency was 47% with a dilute 0.1 mol/kg ethanol solution and the effective distribution coefficient *K* was 0.53 (i.e. the ratio between impurity concentrations in the ice and in the initial solution), whereas with the concentrated 0.3 mol/kg ethanol solution the obtained *K* was 0.36 and separation efficiency 64%. In this case, the average separation efficiency was higher with a more concentrated initial solution.

Table 4. Average properties of ice obtained with ethanol solution concentrations 0.1 and 0.3 mol/kg.

Property	Unit	Ethanol 0.1 mol/kg H_2O	Ethanol 0.3 mol/kg H_2O
Mass growth rate per unit surface area	g/h m^2	748	731
Linear growth rate	m/s	$2.44 \cdot 10^{-7}$	$2.60 \cdot 10^{-7}$
Mass	g	5017	4899
Density	kg/m^3	907.6	-
Natural frequency	Hz	627	-
Thickness	mm	69 (68.05)[1)]	73.33
Average natural frequency per thickness	Hz/mm	9.21	-
Dynamic modulus of elasticity	GPa	7.56	-
Flexural strength	kPa	262	110
Static modulus of elasticity	GPa	1.2	-
Measured initial impurity molality in solution	mol/kg H_2O	0.089	0.292
Impurity molality in ice	mol/kg H_2O	0.047	0.104

[1)] Average thickness from natural frequency measurements

4.3 Average ice properties of sodium chloride solutions

Table 5 shows the average properties for the ice samples formed from 0.1 and 0.3 mol/kg sodium chloride solutions. A comparison of Table 3 to Table 5 shows that the values of mechanical ice properties and ice growth rates for the sodium chloride solution are smaller than for tap water but higher than for the ethanol solution. In general, it was noticed that the ice formed from sodium chloride solutions are mechanically harder than the ice formed from ethanol solutions. The ice formed from a concentrated 0.3 mol/kg sodium chloride solution was mechanically harder (flexural strength 359 kPa) than ice formed from a dilute 0.1 mol/kg ethanol solution (262 kPa), even though the impurity concentration of sodium chloride ice was double when compared with the concentration of ethanol ice, i.e. 0.095 mol/kg vs. 0.047 mol/kg, respectively. The separation efficiency was 71% with a dilute 0.1 mol/kg sodium chloride solution (and the effective distribution coefficient, *K,* 0.29), whereas with a concentrated 0.3 mol/kg sodium chloride solution it was 69% (and *K* 0.31).

Table 5 Average properties of ice obtained with sodium chloride solution concentrations 0.1 and 0.3 mol/kg.

Property	Unit	Sodium chloride 0.1 mol/kg H_2O	Sodium chloride 0.3 mol/kg H_2O
Mass growth rate per unit surface area	g/h m^2	769	710
Linear growth rate	m/s	$2.28 \cdot 10^{-7}$	$2.13 \cdot 10^{-7}$
Mass	g	5158	4768
Density	kg/m^3	961	938
Natural frequency	Hz	362	366
Thickness	mm	64.33 (53.35)[1)]	60.33 (49.13)[1)]
Average natural frequency per thickness	Hz/mm	6.78	7.45
Dynamic modulus of elasticity	GPa	4.82	5.29
Flexural strength	kPa	407	359
Static modulus of elasticity	GPa	4.07	3.26
Measured initial impurity molality of solution	mol/kg H_2O	0.104	0.302
Impurity molality in ice	mol/kg H_2O	0.030	0.095

[1)] Average thickness from natural frequency measurements

4.4 Comparison between the formed ice and to earlier studies

Table 6 depicts the discovered impurities of ice, ice growth rates and mechanical properties

related to properties of tap water ice. The ethanol concentration 0.104 mol/kg in the ice (initial solution 0.3 mol/kg) reduced the flexural strength 90% when compared to the flexural strength of tap water ice. Sodium chloride concentration 0.095 mol/kg in the ice (initial solution 0.3 mol/kg) reduced the flexural strength 67%, while a half lower ethanol concentration 0.047 mol/kg in the ice (initial solution 0.1 mol/kg) generated a 76% strength reduction. Increasing the sodium chloride concentration in the ice from 0.030 mol/kg to 0.095 mol/kg did not have a very noticeable effect on the mechanical rigidity of the ice. The obtained natural frequency per thickness decreased only 9% with 0.047 mol/kg ethanol ice compared to tap water ice. Based on the research, the source of impurity is distinguishable from the differences in the natural frequencies of the ice beams, i.e. the effective stiffness of the ice is at a specific level.

Table 6 Average properties of ethanol and sodium chloride ice compared to properties of tap water ice, samples from rows one to three.

Samples (rows 1 to 3)	Impurity molality mol/kg H_2O	Layer growth[1)]	Mass growth[1)]	Flexural strength[1)]	Static modulus of elasticity[1)]	Natural frequency/ thickness (mech)[1)]	Dynamic modulus of elasticity[1)]
Tap water (P)	-	1.00	1.00	1.00	1.00	1.00	1.00
EtOH 0.1 m (Ea)	0.047	1.04	0.96	0.24	0.32	0.91	0.97
EtOH 0.3 m (Eb)	0.104	1.11	0.94	0.10	-	-	-
NaCl 0.1 m (Sa)	0.030	0.97	0.99	0.38	1.11	0.67	0.62
NaCl 0.3 m (Sb)	0.095	0.91	0.91	0.33	0.89	0.73	0.68

[1)] Related to tap water ice value

The flexural strength results show that tap water ice is the strongest, as expected, and the ethanol solution ice is the weakest. This may partly result from the structure of the ice. As noted in the method description, the beams were assumed to be solid in the calculation of the second moment of inertia as it was not possible to measure the actual porosity. It should be noted that, especially, in the case of ethanol ice, the beams were to solid ice through the thickness and contained pores. Thus, the determined *I* is overestimating the stiffness that leads to the underestimation of the flexural strength in these cases. When compared the

549 studied ice conformations, the structure of tap water ice was the most dense (less porous) and
550 the orientation of the crystals columnar. Ethanol ice had large crystals oriented in different
551 directions, and there were clear regions between the platelets. Thus, the ice was more porous,
552 and concentrated ethanol solution might have been entrapped inside the ice when the platelets
553 were freezing together, i.e. the ice was becoming more dense. The ice from sodium chloride
554 solutions had a structure between these two – the crystals were oriented less randomly and
555 the ice was less porous than the ethanol solution ice but not as dense and even-structured as
556 tap water ice. Thin sections also showed that the crystals of the tap water ice were more
557 rounded, whereas ethanol solution ice had platelet shaped crystals, and sodium chloride
558 solution ice crystal shapes were between these two, see Fig. **6**c and d.
559
560 When these conducted measurements are compared with the previous studies about naturally
561 formed ice in lakes, rivers and seas, the results are reasonable. The tap water represents (in
562 terms of salinity) freshwater ice and the measured values are similar to the values of
563 freshwater ice. The strength of the sodium chloride solutions is similar to lower values of the
564 sea ice strength. Also the static and dynamic elastic modulus values of the tap water and
565 sodium chloride solutions are in the same range as with sea and freshwater ice. The ice grown
566 from the ethanol solution showed higher values than those obtained with fine grained ethanol
567 model scale ice as addressed by Riska et al. (1994). This is reasonable due to structural
568 differences. When the fine grained ethanol ice is produced by spraying, see Von Bock und
569 Polach et al. (2013) the obtained grain size is 1 mm or smaller and the grains are sphere-like.
570 The fracture process occurs along the grain boundaries and by having smaller grain sized ice
571 it leads to weaker ice. Timco (1981)
572
573 Timco (1981) conducted an extensive test series with different aqueous solutions. He noted

574 that the flexural strength decreases as a function of the solute mass fraction increase until a
575 transition concentration point where the ice strength approaches a constant level. The results
576 presented in this paper with sodium chloride solutions are consistent with Timco's results. In
577 the present work, molalities were used for the more accurate comparison of the influence of
578 organic compounds and inorganic salt on ice properties. In addition to mechanical property
579 measurements, the thin sections and structure of obtained ice were presented in this paper,
580 describing the structure of ice more clearly.
581
582 The results show that the average separation efficiency with a 0.3 mol/kg ethanol solution,
583 64%, is higher than with a 0.1 mol/kg ethanol solution, 47%, whereas separation efficiencies
584 with both sodium chloride solutions are at the same level, close to 70%. This peculiar
585 difference in efficiencies could not be noticed within row four ice samples with a higher freezing
586 temperature (-5°C) and therefore induced lower ice growth rates. The separation efficiency
587 with the 0.3 mol/kg ethanol solution was 71% and with 0.1 mol/kg 73%, while with a 0.3 mol/kg
588 sodium chloride solution it was 73% and with 0.1 mol/kg as high as 86%. It is already
589 recognised that higher separation efficiencies can be achieved with lower ice growth rates and
590 dilute solutions (Butler, 2002; Hasan and Louhi-Kultanen, 2015), but no clear explanation for
591 the variation in the ice growth mechanism is known. It might be a result of the structure of the
592 ice in the intermediate stages, i.e. during the growth process, or due to the different properties
593 of the organic (EtOH) and inorganic solutions (NaCl). As this is beyond the scope of this paper,
594 the explanation to this would require additional ice structure studies in relation to ice
595 crystallization kinetics and thermodynamics.

5 Conclusions

The five different initial aqueous solutions – tap water, ethanol and sodium chloride solutions of molalities 0.1 and 0.3 mol/kg – transformed into visually distinguishable ice structures during natural air-cooled freezing. The differences were noticeable also in terms of the conducted chemical and mechanical measurements. Tap water was used as a reference liquid as well as a solvent in ethanol and sodium chloride solutions to compare the properties of the studied ice when ice formed from tap water had the highest flexural strength and natural frequency. The dopants added to the tap water changed the mechanical properties and chemical analysis results of the ice. The platelet diameter and thickness in the intermediate growth stage were the greatest and the orientation was the most random for ice formed from ethanol solutions, which affected the final structure of the ice so that the ethanol ice had the most irregular structure. Based on the research, the ice formed from the ethanol solution is more fragile than the ice formed from the tap water, as the flexural strength is much lower than in tap water ice and sodium chloride ice. Ethanol appeared to weaken the ice more effectively compared to sodium chloride.

In summary, the amount of added chemical dopants, ethanol and sodium chloride, was reduced with variation from 47% to 86% by natural freezing at cooling air temperatures -15°C and -5°C, respectively. This verifies the assumption that higher separation efficiencies can be obtained by lower ice growth rates at higher freezing temperatures, but different chemical characteristics still seem to affect the efficiency level as well. The present study gives a good basis for further research concerning the development of ice harvesting techniques and purification efficiency investigations of freeze separation applications with real wastewaters.

Acknowledgements

The project was funded by the Academy of Finland, project no. 285065, 286184 and 285064. We would like to thank Roman Repin, M.Sc., Ari Tuononen, D.Sc., Mikko Kotilainen, M.Sc., Martin Bergström, PhD, Li Fang, M.Sc., and Mr Teemu Päivärinta for their contribution to the experiments. The earlier contribution of R.U. Franz von Bock und Polach, D.Sc. (Tech.), and Antti Valkeapää, D.Sc. (Tech.), during the research project is also acknowledged.

References

Anderson, D.L., 1958. Preliminary results and review of sea ice elasticity and related studies. Trans. Eng. Inst. Canada 2, 116–22.

Borland, S., 1988. The growth of EG/AD/S model ice in a small tank. OMAE 1988 Houston. Proceedings of the Seventh International Conference on Offshore Mechanics and Arctic Engineering. Vol. 4, pp. 47-53. Arctic engineering and technology. Houston, Texas, February 7-12, 1988.

Butler, M.F., 2002. Freeze concentration of solutes at the ice/solution interface studied by optical interferometry. Cryst. Growth Des. 2, 541-548.

Carvill, J., 1994. Mechanical engineer's data handbook, Butterworth-Heinemann.

Cooling, M., Humphrey, V., Theobald, P. and Robinson, S., 2010. Underwater ultrasonic field characterisation using Laser Doppler Vibrometry of transducer motion. Proceedings of 20th International Congress on Acoustics, ICA 2010.

Dykins, J.E., 1971. Ice engineering: Material properties of saline ice for a limited range of conditions. Tech. Rept. R720. Port Hueneme, CA: Naval Civ. Eng. Lab.

640 Enkvist, E., 1972. On the ice resistance encountered by ships operating in continuous mode
641 of ice breaking. Dissertation. The Swedish Academy of Engineering Science in Finland.
642 Report 24. Helsinki. 181 p.

643 García, V., Häyrynen, P., Landaburu-Aguirre, J., Pirilä, M., Keiski, R.L., Urtiaga, A., 2014.
644 Purification techniques for the recovery of valuable compounds from acid mine drainage
645 and cyanide tailings: Application of green engineering principles. J. Chem. Technol. and
646 Biotechnol. 89, 803-813.

647 Gow, J., Ueda, H., Govoni, J., Kalafut, J., 1988. Temperature and structure dependence of the
648 flexural strength and modulus of freshwater model ice. CRREL Report 88-6.

649 Hammonds, K., Baker, I., 2016. The effects of Ca++ on the strength of polycrystalline ice. J.
650 Glaciol. 62, 954-962.

651 Hammond, N.P., Barr, A. C., Cooper, R. F., Caswell, T. E., Hirth, G., 2018. Experimental
652 constraints on the fatigue of icy satellite lithospheres by tidal forces. J. Geophys. Res.
653 Planets 123 (2), 390-404.

654 Hammonds, K., Baker, I., 2018. The effects of H_2SO_4 on the mechanical behavior and
655 microstructural evolution of polycrystalline ice. J. Geophys. Res.: Earth Surface 123, 535-
656 556.

657 Hasan, M., Louhi-Kultanen, M., 2015. Ice growth kinetics modelling of air-cooled layer
658 crystallization from sodium sulfate solutions. Chem. Eng. Sci. 133, 44–53.

659 Hasan, M., Louhi-Kultanen, M., 2016. Water purification of aqueous nickel sulfate solutions by
660 air cooled natural freezing. Chem. Eng. J. 294, 176-184.

661 Haynes, W.M. (Ed.), 2017. CRC Handbook of Chemistry and Physics. 97th Edition (Internet

662 Version 2017), CRC Press/Taylor & Francis, Boca Raton, FL.

663 Hirayama, K.-I., 1983. Experience with urea doped ice in the CRREL test basin. Proceedings
664 of the 7th Port and Ocean Engineering Under Arctic Conditions Conference, pp. 788-801.
665 Technical Research Center of Finland in Helsinki, April 5-9, 1983.
666 http://www.spri.cam.ac.uk/library/catalogue/records/95170/

667 ITTC guidelines, 2014. Test methods for model ice properties. ITTC Recommended
668 Procedures and Guidelines section 7.5-02-04-02.

669 Kujala, P., Riska, K., Varsta, P., Koskivaara, R., Nyman, T., 1990. Results from in-situ four
670 point bending stress tests with Baltic sea ice. Proceedings of IAHR Ice Symposium, Vol.
671 1. Espoo. pp. 261-278.

672 Lau, M., Wang, J., Lee, C., 2007. Review of ice modeling methodology. In proceedings of Port
673 and Ocean Engineering under Arctic Conditions (POAC). Dalian, China, June 27-30,
674 2007.

675 Lehmus, E., 1988. The properties of EG/AD-model ice in VTT ice basin. Proceedings of
676 Polartech '88. International Conference on Technology for Polar Areas, the Norwegian
677 Institute of Technology. Trondheim, Norway, 15-17 June 1988. Vol. 2, pp. 661-668.

678 Määttänen, M., 1976. On the flexural strength of brackish water ice by in-situ tests. Mar. Sci.
679 Commun. 2, 125-138.

680 Narita, S., Inoue, M., Kishi, S., Yamauchi, Y., 1988. The model ice of the NKK ice model basin.
681 Proc. of the IAHR Ice Symposium. Sapporo, Japan.

682 Nortala-Hoikkanen, A., 1990. FGX model ice at the Masa-Yards Arctic Research Centre.
683 Proceedings of the 10th IAHR International Symposium on Ice. Espoo, Finland, August

20-23, 1990. Vol. 3, pp. 405-408. Helsinki University of Technology.

Parnes, R., 2001. Solid Mechanics in Engineering, 1st edition, Wiley, 728 pp.

Petrich, C., Eicken, H., 2010. Growth, structure and properties of sea ice. In: Thomas, D.N., Dieckmann, G.S. (Eds.), Sea Ice. 2nd Edition, pp. 23-77.

Polytec, 2017. Polytec scanning vibrometer PSV-500 datasheet. Polytec Inc.

Rao, S. S., 2007. Vibration of Continuous Systems. 1st edition, John Wiley & Sons, Hoboken, New Jersey.

Riska, K., Jalonen, R., Veitch, B., Nortala-Hoikkanen, A., Wilkman, G., 1994. Assessment of ice model testing techniques. In proceedings of Ships and Marine Structures in Cold Regions (ICETECH). Calgary, Canada, March 1994.

Schulson, E.M., P. Duval, 2009. Creep and Fracture of Ice. Cambridge University Press Cambridge.

Snyder, S.A., Schulson, E. M., Renshaw, C. E., 2015. The role of damage and recrystallization in the elastic properties of columnar ice. J. Glaciol. 61, 461-480.

Snyder, S.A., Schulson, E. M., Renshaw, C. E., 2016. Effects of prestrain on the ductile-to-brittle transition of ice. Acta Mater. 108, 110-127.

Timco, G., 1980. The mechanical properties of saline-doped and carbamide (urea)-doped model ice. Cold Reg. Sci. and Technol. 3, 45-56.

Timco, G., 1981. Flexural strength of ice grown from chemically impure melts. Cold Reg. Sci. and Technol. 4, 81-92.

Timco, G., 1986. EG/AD/S: A new type of model ice for refrigerated towing tanks. Cold Reg.

Sci. and Technol. 12, 175-195.

Timco, G., Weeks, W., 2010. A review of the engineering properties of sea ice. Cold Reg. Sci. and Technol. 60, 107–129.

Timco, G.W, O'Brien S., 1994. Flexural strength equation for sea ice. CRST 22 (3), 285-98.

Vaudrey, K.D., 1977. Ice engineering: Study of related properties of floating sea-ice sheets and summary of elastic and viscoelastic analysis. US Navy Civil Engineering Lab Rept no TR-860. Port Hueneme, CA.

Von Bock und Polach, R., Ehlers, S., Kujala, P., 2013. Model-scale ice – Part A: Experiments. Cold Reg. Sci. and Technol. 94, 74-81.

Weeks, W.F., Assur A., 1968. The mechanical properties of sea ice. In Proc. Conf. on Ice Pressures Against Structures Tech Memo no 92, Quebec, Laval University, Assoc. Comm. on Geotech. Res., Nat. Res. Council of Canada: 25–78. (CRREL Monograph II-C3.)

Weeks, W.F., Hibler, W. D., 2014. On Sea Ice. University of Alaska Press.

Yasui, M., Schulson, E.M., Renshaw, C. E., 2017. Experimental studies on mechanical properties and ductile-to-brittle transition of ice-silica mixtures: Young's modulus, compressive strength and fracture toughness. J. Geophys. Res. Solid Earth 133, 6014-6030.